scientific reports

OPEN

Distribution equality as an optimal epidemic mitigation strategy

Adar Hacohen[1,2], Reuven Cohen[3], Sol Efroni[2], Ido Bachelet[1] & Baruch Barzel[3,4,5]✉

Upon the development of a therapeutic, a successful response to a global pandemic relies on efficient worldwide distribution, a process constrained by our global shipping network. Most existing strategies seek to maximize the outflow of the therapeutics, hence optimizing for rapid dissemination. Here we find that this intuitive approach is, in fact, counterproductive. The reason is that by focusing strictly on the quantity of disseminated therapeutics, these strategies disregard the way in which this quantity distributes across destinations. Most crucially—they overlook the interplay of the therapeutic spreading patterns with those of the pathogens. This results in a discrepancy between supply and demand, that prohibits efficient mitigation even under optimal conditions of superfluous flow. To solve this, we design a dissemination strategy that naturally follows the predicted spreading patterns of the pathogens, optimizing not just for supply volume, but also for its congruency with the anticipated demand. Specifically, we show that epidemics spread relatively uniformly across all destinations, prompting us to introduce an equality constraint into our dissemination that prioritizes supply homogeneity. This strategy may, at times, slow down the supply rate in certain locations, however, thanks to its egalitarian nature, which mimics the flow of the pathogens, it provides a dramatic leap in overall mitigation efficiency, potentially saving more lives with orders of magnitude less resources.

Global pandemics driven by international mobility[1–6], once an abstract threat, have now, with the advent of COVID-19[7–12], become a realistic scenraio, twards which we must prepare. Originating in a random outbreak, the pathogens spread internationally though air-travel, then locally, at each destination via contagion dynamics[13,14]. When such events transpire, the challenge is to (i) develop ad hoc a drug or vaccine; then (ii) design an efficient strategy for its global dissemination. The point is that even if a therapeutic is avalibale, eliminating challenge (i), we must still ship it to multiple destinations worldwide—potentially stretching our transportation resources to their maximal capacity. Hence, to outrun the epidemic, we crucially need optimal dissemination schemes, that achieve the most efficient mitigation, in the face of limited shipping capacity[15–19].

The common approach to this challenge treats the dissemination as a commodity flow problem[20–23]. The therapeutics (commodity) are shipped from one or few sources, propagating along transportation routes—each with a given shipping capacity—aiming to fill the demand of all network nodes. In this framework one seeks the shipping sequence that optimally utilizes the network—namely, allows for the maximal *volume* of commodity to flow through the network per unit time[24,25] (Fig. 1a). This well-established approach, however, overlooks the interplay between the supply, i.e. the therapeutics, and the demand, here generated by the spreading pathogens. *Indeed, our true goal is not just to generate the maximal outflow of commodities, but rather to obtain the optimal mitigation of the disease*. This does not depend only on the *volume* of commodity flow, but also on the manner in which this volume is distributed across all potential destinations, i.e. its *spreading pattern*[26,27]. Consequently, the most efficient shipping sequence might be one that compromises maximal flow, but generates the optimal spreading patterns, compatible with those of the pathogens[13,28–30].

With this in mind, we take here a network dynamics approach, and analyse the spatiotemporal propagation patterns[26,27] of both the commodities and the pathogens (Fig. 1b). We find that while the disease impacts the majority of nodes uniformly, maximum commodity flow optimization naturally yields a highly uneven spread, conflicting a concurrent and homogeneous global demand with an extremely heterogeneous supply pattern. This discrepancy, we find, is not merely theoretical, but, in fact, it was clearly evident during COVID-19. There, comparing the epidemic vs. vaccine spreading patterns we observe precisely the predicted mismatch. As a result of this supply/demand incompatibility, not only does maximum flow not guarantee optimal mitigation, it is, in fact, counterproductive, indeed, generating a desirable *volume* of available therapeutics, but at the same time a highly undesirable *spreading pattern*.

[1]Augmanity, Rehovot, Israel. [2]Faculty of Life Sciences, Bar-Ilan University, Ramat Gan, Israel. [3]Department of Mathematics, Bar-Ilan University, Ramat Gan, Israel. [4]The Gonda Multidisciplinary Brain Research Center, Bar-Ilan University, Ramat Gan, Israel. [5]Network Science Institute, Northeastern University, Boston, MA, USA. ✉email: baruchbarzel@gmail.com

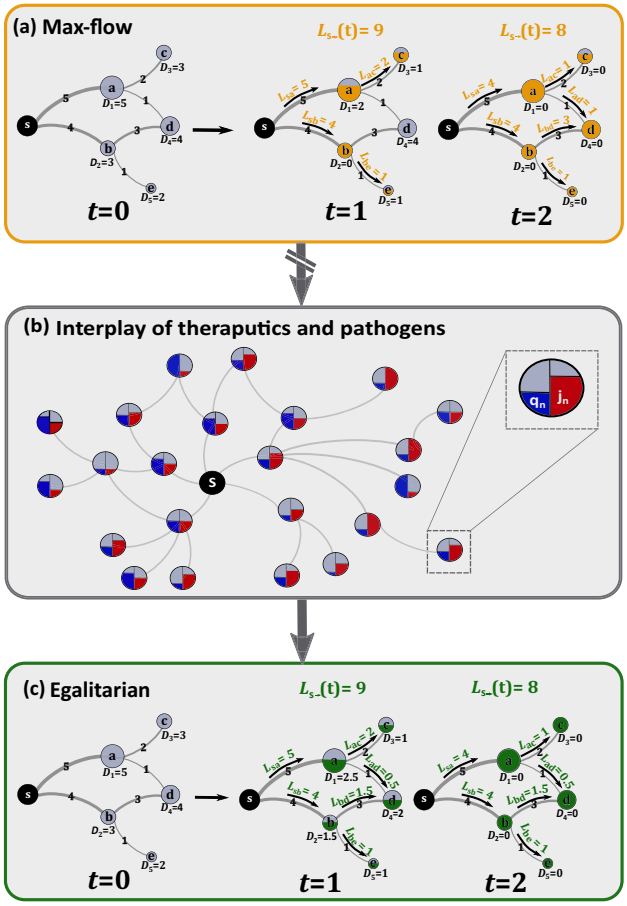

Figure 1. Optmizing therapeutic dissemination for efficient mitigation. We treat the theraputic spread as a commodity flow problem. (**a**) Commodities flow from the source s to fill the demands $D_n(t)$ at all destinations a through e. The transportation network imposes constraints, expressed by the restricted shipping capacity of all links. For example, the route $s \to a$ can transport at most 5 units per day (edge labels). The shipping sequence determines the quotas shipped via each link L_{nm}, and hence the rates by which all nodes are supplied. Demands are updated as therapeutics are supplied—for instance, at $t = 1$ b's demand $D_2(t)$ is updated to zero, as b's quota is filled. Under max-flow the goal is to achieve the highest net outflow of commodities from s, i.e. maximize $L_{s\to}(t)$. Here, nodes were supplied within 2 days, a net flow $L_{s\to}(1) = 9$ in day 1 and $L_{s\to}(t) = 8$, in day 2. (**b**) During an epidemic, however, the goal is to achieve optimal mitigation, not just optimal commodity flow. This requires us to consider the interplay between our dissemination and the spread of the epidemic. Each node's demand is determined by its infection levels ($j_n(t)$, red), leading us to seek the shipping sequence which best adresses the anticipated spread of infections—aiming for supply ($q_n(t)$, blue) that is most compatible with demand. (**c**) We find that the optimal strategy is to design an egalitarian flow, in which supply is homogeneously spread across all destinations. Using the same network as in (**a**), our egalitarian strategy yields a balanced shipping sequence, in which nodes are supplied concurrently at roughly equal rates. For example, instead of fully supplying node b in $t = 1$ and only then shipping to d at $t = 2$, as done under max-flow in (**a**), our egalitarian algorithm favors the shipping sequence where b and d are simulataneasly supplied at equal rates. Under global demand, we show, such egalitarian supply is orders of magnitude more effective in terms of mitigation and resource disposal.

To solve this, we introduce an *equality* criterion into the optimization, that prioritizes dissemination sequences with homogeneous spreading patterns (Fig. 1c). This ensures that the therapeutic flow is not just rapid, but also properly disseminated, generating supply patterns that are compatible with demand. The resulting dissemination, we find, is orders of magnitude more efficient, achieving higher mitigation levels even under extremely prohibitive shipping constraints. We examine our strategy, first on a set of hypothetical epidemic scenarios, which allow us to extract analytical insights, and then on a COVID-19 inspired simulation, where we assess the practical relevance of our analysis. Our strategy is tailored primarily towards drug-based mitigation, offering guidelines for the future dissemination of currently produced therapies[31]. Yet, as we explain below, it is also relevant for vaccine distribution.

Mitigation via maximum-flow

To examine our response to a global epidemic, we begin by considering different epidemiological scenarios, from mildly contagious to extremely transmissible, in which a disease spreads globally via air-travel, under the susceptible-infected-recovered (SIR) epidemic model[13,14,32] (Box 1). We used empirical data on human aviation to evaluate the flux of passengers between 1292 local populations (nodes), each with M_n individuals ($n = 1, \ldots, N$), and quantified the impact of the epidemic through its global *coverage*

$$R(t) = \frac{1}{\Omega}\sum_{n=1}^{N} M_n r_n(t), \tag{1}$$

where $r_n(t)$ is the fraction of recovered individuals in n and $\Omega = \sum_{n=1}^{N} M_n$ represents the global population. Hence, $R(t)$ in (1) captures the fraction of impacted individuals worldwide. In Fig. 2a we show the unmitigated $R(t)$ under three different scenarios: extremely contagious, where $R(t \to \infty) \to 1$ (dark red), medium ($R(t \to \infty) \approx 0.5$, red) and mild ($R(t \to \infty) \approx 0.3$, light red).

Following the initial outbreak at $t = 0$, we define the response time t_R as the time required to begin the distribution of a therapy. This therapy can be in the form of a vaccine, designed to prevent the infection of *susceptible* individuals, or a drug, facilitating the recovery of *infected* individuals. As we consider a scenario in which the disease is rapidly spreading, and hence many individuals may already be infected, we focus below on the dissemination of drugs, which remain relevant at all stages of the spread[33,34].

Focusing on the efficiency of *dissemination*, rather than production, we assume that the therapeutic is already stockpiled in sufficient quantities at a specific source node s. Therefore, the main challenge is to optimally distribute it via the air-transportation network to all destinations. The network is characterized by the *carrying capacities* B_{nm} that quantify the daily volume of drugs that can be shipped through each air-route $m \to n$, i.e. $B_{nm} = B_{n\leftarrow m}$. The challenge is, therefore, to obtain the optimal shipping sequence from s to all other nodes, under the constraints imposed by B_{nm}.

Max-flow mitigation (Fig. 2a–c). In the maximum flow dissemination strategy we seek to maximize the daily volume of drug doses spreading from s to the rest of the network. Denoting the number of doses shipped from m to n on day t by $L_{nm}(t)$, our optimization translates to

$$\textbf{Maximize}\{L_{s\to}(t)\} \tag{2}$$

where

$$L_{n\to}(t) = \sum_{m=1}^{N}(L_{mn}(t) - L_{nm}(t)), \tag{3}$$

captures the net daily outflow of drugs from n. Hence, in Eq. (2), by maximizing $L_{s\to}(t)$, i.e. the outflow from the source, we seek to boost the total volume of drugs introduced into the network in each day. This maximization is subject to two constraints:

$$0 \le L_{nm}(t) \le B_{nm} \;\text{ for all }\; n, m = 1, \ldots, N \tag{4}$$

$$0 \le L_{n\leftarrow}(t) \le D_n(t) \;\text{ for all }\; n = 1, \ldots, N, n \ne s\,. \tag{5}$$

The first constraint (4) ensures that the daily flux along each route $m \to n$ is within the bounds of the route carrying capacity B_{nm}. The second constraint (5) restricts nodes from accumulating doses in excess of their remaining demand at time t. Hence n's net *incoming* flux $L_{n\leftarrow}(t)$ is bounded by n's current demand, $D_n(t)$; note that $L_{n\leftarrow}(t) = -L_{n\to}(t)$.

We consider three strategies for setting the demands: (i) *Population-based*. At $t = 0$ we set $D_n(0)$ to be proportional to each node's population M_n, then update these demands daily according to n's supply, as $D_n(t+1) = D_n(t) - L_{n\leftarrow}(t)$ (ii) *Impact-based*. Setting $D_n(0)$ according to the projected number of infected individuals at n (iii) *Urgency-based*. Updating $D_n(t+1)$ dynamically based on n's supply gap at t, such that highly impacted (or undersupplied) nodes are prioritized. While (i) is simplest, it is also inefficient, tending to overestimate the actual demand at n; strategy (iii), on the other hand, is highly complex, relying on real-time tracking and updating of the demands, but, in some cases, benefits, by design, from a high level of congruency with the spread of the pathogens. An expanded discussion of these three strategies appears in Supplementary Section 2.4.

Network capacity. Applying (2)–(5), the maximal dissemination rate one can achieve is restricted by the out-degree of the source node, $K_s = \sum_{n=1}^{N} B_{ns}$, representing an upper-bound on the volume of drugs that can be introduced into the network per day. We, therefore, define the network's normalized *capacity* with respect to each source s as

$$C_s = \frac{K_s}{\Omega}, \tag{6}$$

normalized to $C_s = 1$ in case s can disseminate sufficient doses to meet the entire global demand (Ω) in 1 day. The network capacity can be controlled by rescaling all individual carrying capacities B_{nm}, to describe affluent vs. restrictive dissemination scenarios (Supplementary Section 2.3).

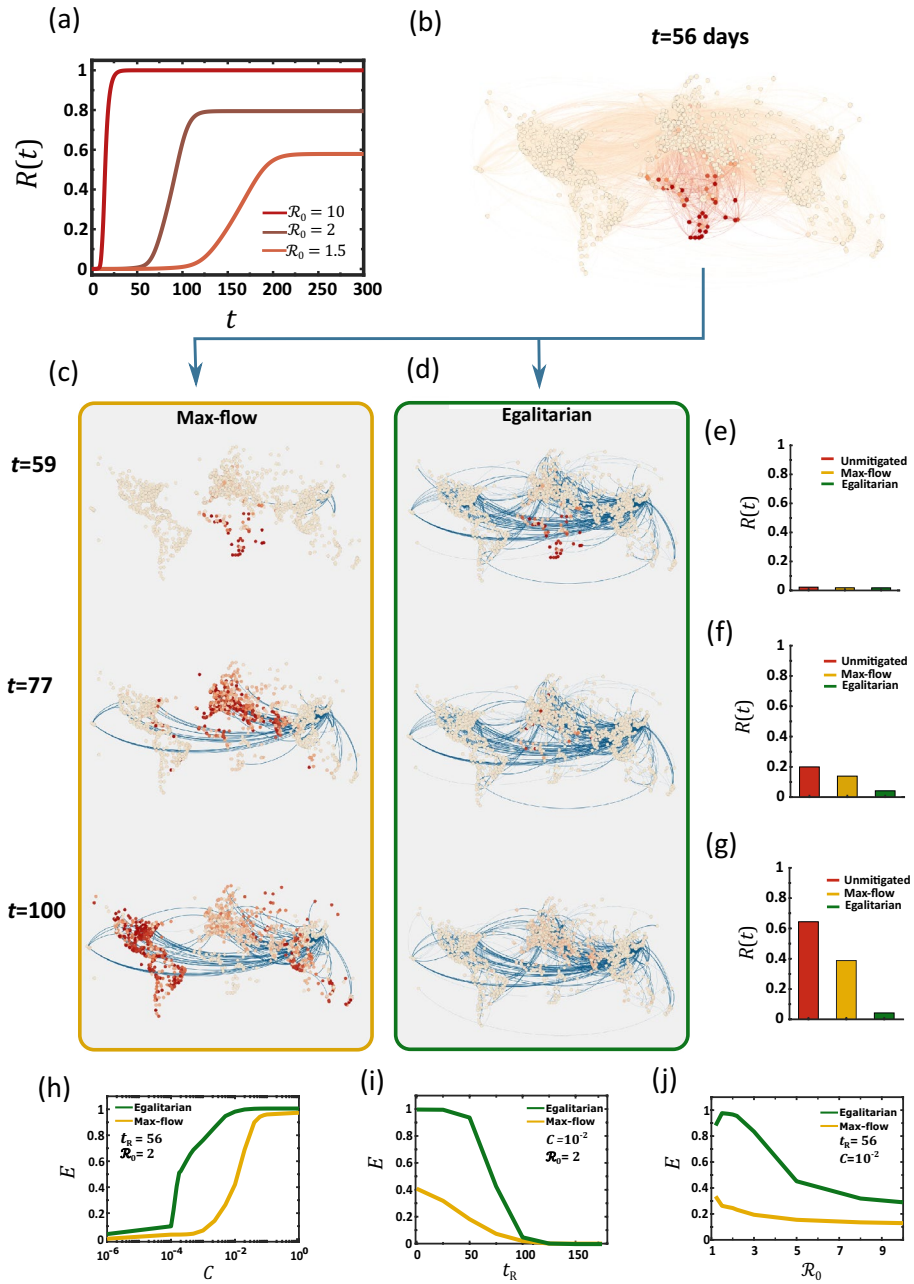

Figure 2. Outrunning a contageuous epidemic using max-flow vs. egalitarian dissemination. (**a**) The global coverage $R(t)$ vs. t following an outbreak at Burundi (BJM) under three scenarios: severe (dark red $\mathcal{R}_0 = 10$), intermediate (red, $\mathcal{R}_0 = 2$) and mild (light red, $\mathcal{R}_0 = 1.5$). (**b**) The state of the epidemic (under $\mathcal{R}_0 = 2$) at $t = 56$ days, directly before drug dissemination begins. The local coverage $r_n(t)$ in each node and the flux of infected individuals along each link (air-route) are represented by their red color depth. (**c**) *Max-flow dissemination*: starting at $t_R = 56$ we begin drug dissemination from Osaka (ITM) via max-flow; Eqs. (2)–(5). Drug fluxes $L_{nm}(t)$ (links) and drug availability $q_n(t)$ (nodes circumference) are represented by blue color depth. We observe a *race* between the therapeutic and the disease, both spreading along similar routes, ending in a significant fraction of infected individuals, as indicated by the prevalence of red nodes at $t = 100$. (**d**) *Egalitarian dissemination*: under the same scenario, the egalitarian strategy of Eqs. (12)–(14) achieves a much more efficient mitigation, where by $t = 100$, the epidemic is almost eliminated. (**e**)–(**g**) $R(t)$ at the three time-points for the unmitigated spread (red), under max-flow (yellow) and under egalitarian (green). By $t = 100$ egalitarian has reduced the global coverage by a factor of ~ 20, from $R(t) = 0.65$ to $R(t) = 0.04$, while max-flow has achieved a mere ~ 1.5 factor reduction. Three crucial parameters may impact our mitigation: the global transportation capacity C, our response time t_R and the severity of the contagion $\mathcal{R}_0$. (**h**) Mitigation efficiency E vs. C under egalitarian (green) and max-flow (yellow). The former achieves higher efficiency with orders of magnitude less resources. For example, egalitarian provides $E = 0.8$ under $C \sim 10^{-3}$, as compared to $C \sim 10^{-1}$, a two order of magnitude gap, required under max-flow for similar efficiency. (**i**) E vs. t_R. Again, we find that egalitarian shows a significantly higher performance in the face of a late response. (**j**) E vs. $\mathcal{R}_0$, confirming, again, the consistent advantage of egalitarian mitigation. In each panel we vary one parameter and list the set values of the other two.

In Fig. 2b,c we present the evolution of the epidemic at four selected time-points. At $t = 0$ we simulate an outbreak (red) at Burundi (BJM), emulating the 2013 Ebola, which originated in Africa[35,36], then track its spread through air-travel, setting $\mathcal{R}_0 = 2$. The node infection levels and the epidemic fluxes, i.e. the daily volume of infected passengers on each route, are represented by red color depth. Drug dissemination via max-flow optimization (blue) begins at $t_R = 57$ days in Osaka (ITM), using blue color depth to signify the availability/flux of drugs in each node/route. We set the network capacity in Eq. (6) to $C = 10^{-2}$, a dissemination capability of 1% of the global demand per day, and assign demands $D_n(t)$ using the impact-based strategy. We find, through the long-term prevalence of infections (Fig. 2c, red), that under these conditions, mitigation falls short. Indeed, in Fig. 2e–g we observe that the coverage $R(t)$ in (1) is only slightly affected by our max-flow mitigation (red vs. yellow), illustrating the failure to effectively suppress the epidemic.

For a more systematic assessment of our dissemination strategy, we track the mitigation efficiency via[15]

$$E = 1 - \frac{R_\infty(C)}{R_\infty(0)}, \tag{7}$$

where $R_\infty(C)$ is the long term coverage of the epidemic, i.e. $R(t \to \infty)$, under mitigation with network capacity $C_s = C$. Efficient mitigation has $R_\infty(C) \ll R_\infty(0)$, capturing a significant reduction in the disease coverage, which in (7) translates to $E \to 1$. Conversely, a failed mitigation leaves infection levels almost unchanged, leading to $E \to 0$. Testing E vs. C under maximum flow dissemination, we find that for a broad range of C levels the epidemic is almost unaffected, a consistently inefficient mitigation in which $E \ll 1$ (Fig. 2h, yellow). Effective mitigation is only achieved around $C \gtrsim 0.1$, a limit in which s is capable of shipping doses in the order of the entire global demand in just a few days. Such optimal conditions are not only unlikely, but mainly, they indicate the inefficiency of this dissemination strategy, requiring an extreme volume of therapeutics shipped in a highly constrained timeframe in order to achieve a measurable impact on the epidemic.

It seems, therefore, that the max-flow optimization strategy is inadequate for the containment of a globally spreading epidemic. In Supplementary Section 2 we analyze the population and urgency-based strategies, observing similar challenges.

The roots of the max-flow inefficiency

Our mitigation is, in its essence, a spreading competition between the therapeutics and the pathogens, both progressing along the same underlying network, i.e. air-transportation[19]. It seems, therefore, that winning this competition is a matter of shipping capacity: we must generate sufficient therapeutic fluxes to outrun the spread of the disease, namely we must increase C_s. However, the analysis above indicates, that there is an intrinsic deficiency in the spread of therapeutics, that cannot be easily compensated by simply increasing shipping rates. Next, we show that the real challenge is rooted in the fact that the two competing processes—epidemics vs. therapeutics—lead to fundamentally different spreading patterns, in which the pathogens benefit from an intrinsic advantage.

Propagation of pathogens (Fig. 3a,b). Pathogens spread via diffusion coupled with local SIR dynamics, as captured by Eqs. (16) in Box 1. In this process, upon penetration of node n, the pathogens reproduce locally through SIR, until reaching peak infection at $t = T_n^{\mathrm{P}}$. In a network environment, since the majority of nodes are at the mean distance from the initial outbreak, we find that after a limited propagation time, most nodes reach peak infection approximately simultaneously. We track this via the infection rate

$$\mathbb{I}_n = \frac{1}{T_n^{\mathrm{P}}}, \tag{8}$$

capturing the average *speed* by which the pathogens propagate to n. In Fig. 3b we show $P(\mathbb{I})$, the probability density for a randomly selected node n to have $\mathbb{I}_n \in (\mathbb{I}, \mathbb{I} + \mathrm{d}\mathbb{I})$. Indeed, we find that $\mathbb{I}_n$ follows a bounded distribution, where the majority of nodes are infected at a similar rate, and hence their peak infection occurs at roughly the same time. Such uniform propagation patterns lead to a simultaneous global peak infection, and, as a consequence, to a concurrent global demand for therapeutics.

Dissemination of therapeutics (Fig. 3c,d, Supplementary Section 4). The dynamics of commodity flow, as provided by Eqs. (2)–(5) are fundamentally different. The therapeutics flow from a single source node s, and undergo dilution as they disperse across the exponentially growing number of pathways[37,38]. Such flow patterns naturally lead to a highly heterogeneous supply pattern across all nodes. To observe this we consider the therapeutic supply time T_n^{S} for node n to fill its therapeutic demand, and its subsequent supply *rate*

$$\mathbb{S}_n = \frac{1}{\Delta t_n}, \tag{9}$$

where $\Delta t_n = T_n^{\mathrm{S}} - t_{\mathrm{R}}$, is the elapsed time from initial dissemination (t_{R}) to n's final supply (T_n^{S}). This rate $\mathbb{S}_n$ quantifies how rapidly n receives treatment. In Supplementary Section 4 we show that under max-flow mitigation the probability density $P(\mathbb{S})$ follows a power law of the form

$$P(\mathbb{S}) \sim \mathbb{S}^{-\nu}, \tag{10}$$

with $\nu = 2$ (Fig. 3d). Hence, in contrast to the homogeneity of the *pathogen* spread, *supply* is extremely heterogeneous, with a vast majority of undersupplied nodes (small $\mathbb{S}_n$, shaded 80%), and a selected privileged minority of well-treated destinations (large $\mathbb{S}_n$).

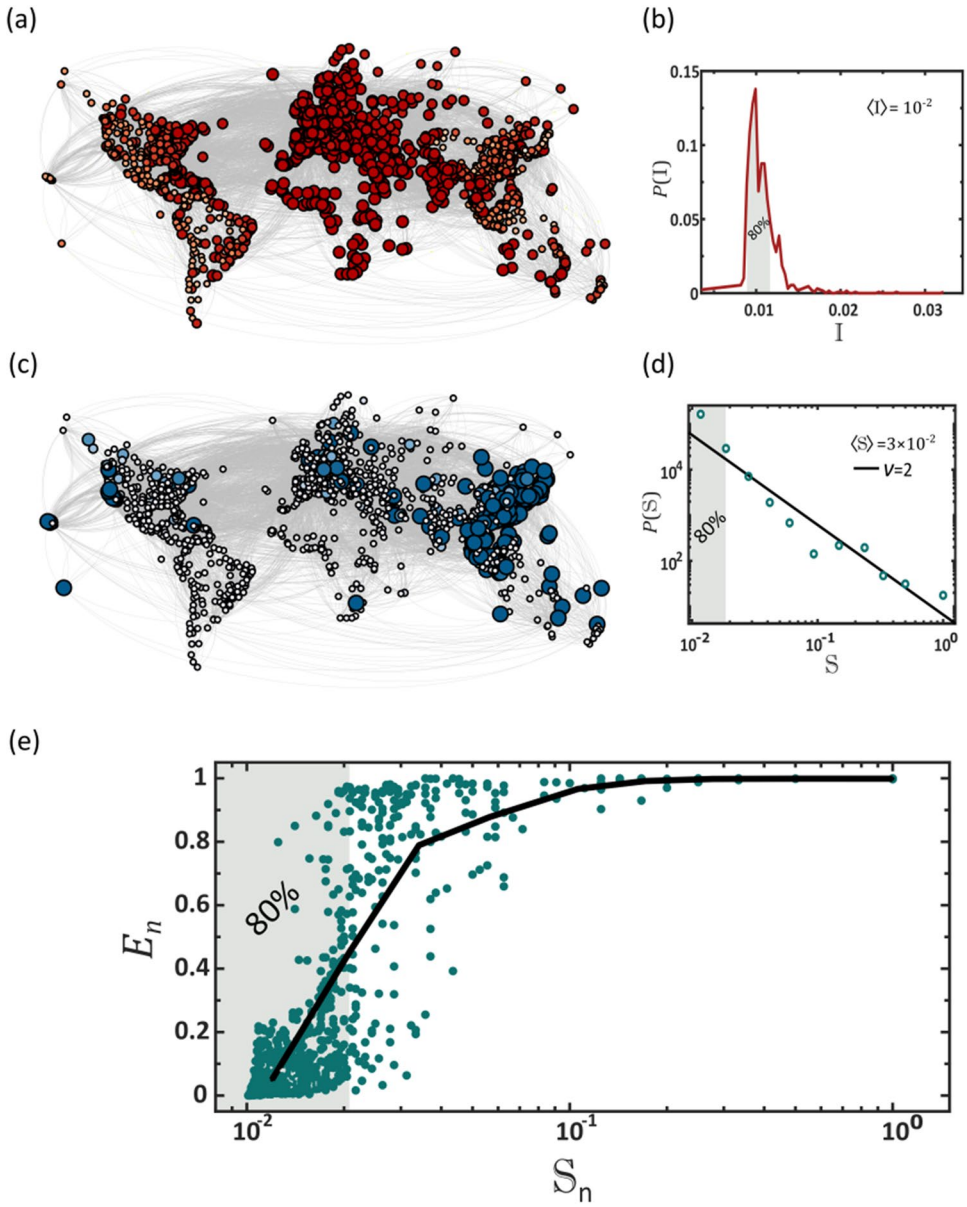

Figure 3. Why max-flow provides sub-optimal mitigation. (**a**) Pathogens spread via contagion dynamics, reproducing in each desination independently via the SIR process. The result is a relatively homogeneous spread, in which the majority of destinations reach peak infection (red) at approximately the same time. Here this is observed by the almost uniform red shade and size of all nodes, capturing the instantaneuous infection levels $j_n(t)$ during the time of global peak infection. (**b**) To quantify this we measure the infection rate $\mathbb{I}_n$ of all nodes as obtained from Eq. (8), and plot its distribution $P(\mathbb{I})$. The bounded form of $P(\mathbb{I})$ indicates the homogeneous nature of the pathogen spread. Indeed, we find that 80% of the nodes are impacted wthin a small margin around the average (shaded area). (**c**) Using max-flow we track the availability of the therapeutics $q_n(t)$ at all destinations (node size/blue color depth). In contrast to the pathogens, the therapeutics naturally spread extremely unevenly, with a small minority of early supplied nodes (large, dark blue), coexisting alogside a majority of delayed destinations (small, light blue). (**d**) The supply rate distribution $P(\mathbb{S})$ as obtained via max-flow (circles). As predicted in Eq. (10), $P(\mathbb{S})$ can be approximated by a power-law $P(\mathbb{S}) \sim \mathbb{S}^{-\nu}$, with $\nu = 2$ (solid line). This captures an extremely heterogeneous dissemination pattern, in which 80% of the nodes are supplied at a below average rate (shaded area). Hence, max-flow confronts a homogeneous demand ($j_n(t)$, red) with an extremely hetergeneous supply ($q_n(t)$, blue). (**e**) The local efficiency E_n vs. supply rate $\mathbb{S}_n$ as obtained via max-flow dissemination. As expected we find that $\mathbb{S}_n$ crucially impacts the mitgation effectiveness at n. Therefore, the fat-tailed nature of $P(\mathbb{S})$, in which the majority of nodes have a small $\mathbb{S}_n$ (80%, shaded) creates an intrinsic mitigation defficiency, in which most destinations experience insufficient supply. The challenge, we emphasize, is not in the production/shipping capacities, as indeed we have $\langle \mathbb{S} \rangle \approx \langle \mathbb{I} \rangle \approx 10^{-2}$, namely, that on average, supply rate can meet the evolving demand. Rather, is is rooted in the patterns of spread of the existing supply, which are fundamentally incongruent with those of the pathogens.

Together, this combination of *homogeneous* demand and *heterogeneous* supply, a consequence of the naturally occurring spreading patterns of pathogens versus commodities, creates a crucial gap in our ability to effectively mitigate a global pandemic. To understand this, consider ideal flow conditions, where $\langle \mathbb{S} \rangle > \langle \mathbb{I} \rangle$, namely that, on average, drug dissemination is more rapid than the pathogen propagation. Still, the fat-tailed nature of $P(\mathbb{S})$ vs. the bounded form of $P(\mathbb{I})$ indicates that while most nodes have $\mathbb{I}_n \approx \langle \mathbb{I} \rangle$, when it comes to supply, the typical node has $\mathbb{S}_n < \langle \mathbb{S} \rangle$. Indeed, in a scale-free distribution the majority of entries are below the mean. This is illustrated in Fig. 3, where we show that 80% of nodes are within a 20% margin of $\langle \mathbb{I} \rangle$, i.e. they are all impacted within a narrow time window around the mean (Fig. 3b, shaded). Yet, in contrast, a similar 80% have a therapeutic rate below $\langle \mathbb{S} \rangle$, i.e. they witness supply deficiency (Fig. 3d, shaded). Hence we are confronted with a reality in which almost all nodes require treatment, and yet only a small minority receives sufficient, and at times, even superfluous, supply.

This uneven distribution $P(\mathbb{S})$ directly impacts our mitigation efficiency. To observe this, consider the local efficiency

$$E_n = 1 - \frac{r_{n,\infty}(C)}{r_{n,\infty}(0)}, \tag{11}$$

where $r_{n,\infty}(C) = r_n(t \to \infty)$ under mitigation with capacity $C_s = C$. While E in (7) captures the global mitigation efficiency, E_n focuses specifically on the effect observed at n, hence quantifying n's local benefit from the supplied drugs. In Fig. 3e we show E_n vs. $\mathbb{S}_n$. As predicted, we observe that $\mathbb{S}_n$ is a crucial determinant of mitigation efficiency. Indeed, nodes with low $\mathbb{S}_n$ (shaded), by far the majority of nodes thanks to the power-law structure of $P(\mathbb{S})$, exhibit an almost vanishing E_n. This illustrates, once again, the flaw of max-flow: most nodes, the deprived 80%, have $E_n \to 0$, while a small minority benefit from $E_n \to 1$.

Taken together, our analysis shows that the common approach of maximizing flow is insufficient, as it treats the *mean* flow, but not its *distribution*. Most essentially, it disregards the interplay with the competing flow of the pathogens. The crucial point it that the main challenge is rooted in *equality* ($P(\mathbb{S})$) rather than in *quantity* ($\langle \mathbb{S} \rangle$), namely not the volume of the outflux, $L_{s\to}(t)$, but rather the way in which this volume distributes across the network. Hence, below, in addition to max-flow, we also optimize for supply homogeneity.

Optimizing for homogeneity

Egalitarian mitigation (Fig. 1c). The optimization of Eqs. (2)–(5) is designed to increase the volume of drugs introduced into the network, but as we have shown, it leads to an extremely sub-optimal dispersion pattern. To remedy this, we introduce a homogeneity criterion, replacing the maximization in (2) by (Supplementary Section 2)

$$\textbf{Maximize}\left\{ L_{s\to}(t) + H \sum_{n=1}^{N} \lambda(t) D_n(t) \right\}, \tag{12}$$

where the homogeneity coefficient H determines the relative balance between our optimization for max-flow ($L_{s\to}(t)$) vs. our demand for egalitarian spread ($\lambda(t)$). In addition to constrains (4) and (5) above, we now also require

$$L_{n\leftarrow}(t) \geq \lambda(t) D_n(t) \;\text{ for all }\; n = 1, \ldots, N, n \neq s \tag{13}$$

and

$$0 \leq \lambda(t) \leq 1, \tag{14}$$

forcing, at each step, to supply, at the least, a fraction $\lambda(t)$ of every node's current demand. This strategy seeks to maximize flow, but at the same time favors solutions that supply all nodes simultaneously. Indeed, constraint (13) prohibits shipping sequences that at any step supply exclusively a subset of the nodes. This additional constraint may, in general, lead to a diminished net flow, however, thanks to its egalitarian nature, we find that it dramatically enhances mitigation efficiency.

To observe this, we revisit the epidemic spread of Fig. 2, leaving all conditions unchanged, except that now, instead of the max-flow optimization of (2)–(5) we mitigate the disease via the egalitarian strategy of (12)–(14). The results are striking: egalitarian dissemination practically eliminates the epidemic, as observed by the dominance of blue nodes/links at $t > t_R$ (Fig. 2d). Indeed, compared to the $\sim$ 30% reduction in $R(t \to \infty)$ afforded by max-flow, egalitarian achieves, under the same capacity C_s, a $\sim$ 95% reduction, representing a practically perfect mitigation (Fig. 2g, yellow vs. green).

A systematic comparison of the two mitigation strategies consistently supports the crucial role of dissemination homogeneity. In Fig. 2h we show the efficiency E in (7) vs. C under egalitarian dissemination (green). We find that E approaches 80% already at $C \sim 10^{-3}$. This represents an extreme case of supply deficiency, and yet it affords us a rather desirable outcome. A similar E under max-flow was only observed for $C_s \sim 10^{-1}$ (yellow), a two order of magnitude advantage for egalitarian.

A crucial factor impacting our mitigation efficiency, is the response time t_R, required to identify the threat and initiate a response. To observe this, in Fig. 2i we present E vs. t_R for both max-flow (yellow) and egalitarian (green) mitigation. As expected, we find that E declines with t_R, however, for the entire range of response times egalitarian consistently outperforms max-flow. In Fig. 2j we further show that the egalitarian advantage is consistently maintained for a range of contagion levels $\mathcal{R}_0$.

Hence, examined against a series of potential challenges, from the disease parameters ($\mathcal{R}_0$) to the performance level of our response (t_R, C_s), we find that egalitarian allows enhanced mitigation, in some cases, by a

dramatic margin. This, again, is thanks to egalitarian's homogeneous dissemination patterns, which, at the price of a potentially diminished supply *rate*, afford us a more desirable supply *distribution*, and consequently, an optimized mitigation.

The roots of the egalitarian advantage. The efficiency of egalitarian mitigation may seem, at first glance, implausibly high. For example, Fig. 2h indicates that effective mitigation is already achieved with capacity as low as $C \sim 10^{-3}$ day^{-1}. This represents an extreme scenario, in which we require an order of 10^3 days to supply the global demand, a time-scale that by far exceeds the final spread of the epidemic. Such extraordinary efficiency is rooted in the fact that even a tiny influx of drugs introduced at an early enough stage of the epidemic can dramatically impact its future development.

To understand this, consider a node n at the early stages of the spread, when $j_n(t) \ll 1$. As time advances, this small seed of infections reproduces until n reaches its final infection levels $r_n(t \to \infty)$. Suppressing this seed when it is small is, therefore, the optimal strategy, allowing us, with a tiny supply of therapeutics, to eliminate not just the current $j_n(t)$, but also terminate its potential future reproduction. Hence, maintaining a continuous influx of therapeutics, even at a very low rate, keeps $j_n(t)$ subdued, never allowing the local infections to reach their potential coverage. Egalitarian mitigation is precisely designed to provide such supply patterns: instead of rapidly supplying a select group of nodes at a time, it favors a slow influx that is spread evenly across all nodes, starting from the *get-go* at $t = t_R$.

In contrast, max-flow generates a similar (or even higher) total flux, but spreads it out sequentially—few nodes receive all their supply early on, and are hence successfully treated, while the majority fill their demand at a much later time, when $j_n(t)$ is already harder to contain. To observe this, we revisit the simulated mitigation of Fig. 2, this time focusing on a pair of specific nodes (Fig. 4a): SDJ which is among the few early supplied nodes ($\mathbb{S}_{SDJ} = 0.2$, red), and CGQ, a typical node that represents the majority of destinations, which receive their supply later on ($\mathbb{S}_{CGQ} = 3 \times 10^{-3}$). In Fig. 4b,c we show the drug availability $q_n(t)$ in both nodes (blue), together with their unmitigated (red) vs. mitigated (yellow) disease coverage. Indeed, we find that early supply is crucial, with SDJ benefiting from an almost perfect mitigation, and CGQ being almost unaffected by the late arriving drugs.

Under egalitarian mitigation the supply pattern is fundamentally different. Here, as per the equality constraint, both nodes settle for the *slower* rate $\mathbb{S}_{SDJ} \approx \mathbb{S}_{CGQ} \approx 10^{-3}$. Hence, egalitarian provides no overall rate advantage, and, in fact, disadvantages the previously privileged SDJ. However, now, instead of $q_n(t)$ remaining idle and then, in due time, receiving a sharp supply boost, it is continuously supplied from the outset at t_R (Fig. 4d,e), a direct consequence of the homogeneity constraint of (12)–(14). The advantage is that now both SDJ and CGQ receive treatment early on, mitigating the disease while it is still small, and thus suppressing its potential growth.

Therefore, while egalitarian impedes the supply of the high rate minority, it still allows us to successfully treat both that minority and the low rate majority. This is because its simultaneous, even if slow, supply, affords early treatment for *all* nodes, overcoming $j_n(t)$ while it is still at its embryonic stage.

Mitigation under restricted supply. A crucial implication of the above analysis touches on the global resources required for mitigation[39,40]. Clearly, if we run the max-flow/egalitarian algorithm until all demands are filled, we will inevitably arrive at a total cost of $\sim \Omega$ drug units, supplied at a time-scale of $\sim \Omega/C_s$ days. However, since egalitarian begins supplying all nodes while $j_n(t)$ is still small, it has the potential to overcome the pandemic even before all initial demands $D_n(0)$ are completely satiated. To observe this, we run both strategies—max-flow and egalitarian—for a limited time, from $t = 0$ to T. We then measured the efficiency E (7), in function of the total resource consumption

$$Q(T) = \frac{1}{\Omega}\int_0^T L_{s\to}(t)\mathrm{d}t. \tag{15}$$

Equation (15) quantifies the total outflux of therapeutics from s as a fraction of the global demand Ω, throughout the mitigation period $0 \le t \le T$. The greater is $Q(T)$, the more therapeutic resources that are consumed. As predicted we find in Fig. 4g that egalitarian, not only provides a higher mitigation efficiency, but achieves this in a fraction of the resources. For max-flow (yellow) we observe a linear gain with Q, reaching peak efficiency only around $Q \to 1$, i.e. when supply fills *all* demands. Egalitarian, in contrast, thanks to its simultaneous treatment of all nodes, suppresses the epidemic early on, when it is still manageable, with limited supply. Therefore it enables mitigation above 90% (grey dashed line) with total consumption as low as $Q \sim 0.1$, i.e. a mere 10% of the global demand.

COVID-19 mitigation

Our discussion, up to this point focused on a hypothetical scenario, designed to help us best compare the two contending dissemination strategies, max-flow vs. egalitarian. We, therefore, assumed ideal conditions, where, aside from our drug dissemination, all else remains unchanged, i.e. no lockdowns or travel restrictions. In reality, however, as clearly observed during the spread of COVID-19, our mitigation, hitherto based on vaccines rather than drugs, is also reinforced by reduction in international travel, regional lockdowns, testing and other social distancing practices. As a result, the spreading patterns, characterized by global waves of infection, are highly distinct from the *clean* SIR dynamics of Box 1.

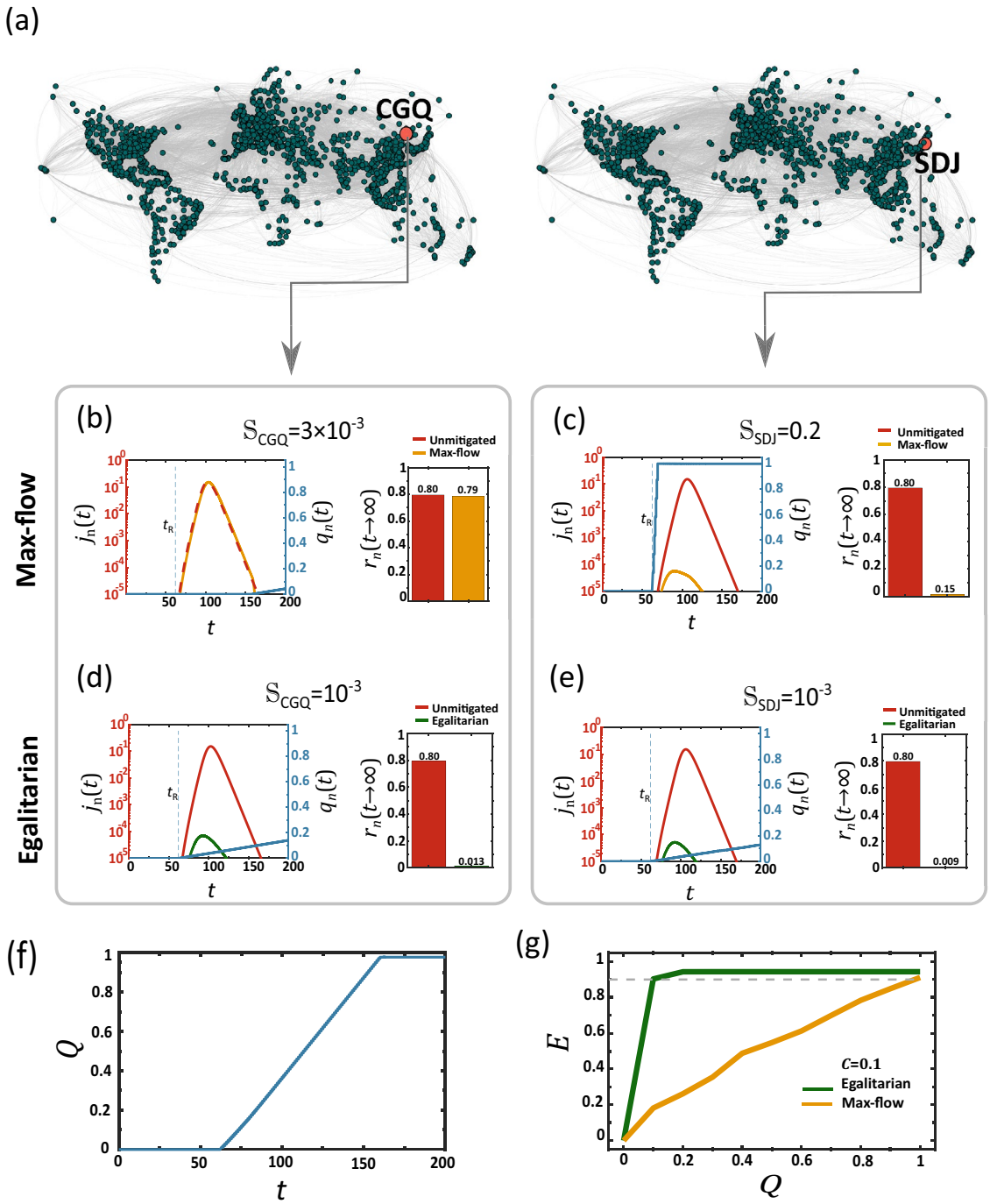

Figure 4. The roots of the egalitarian advantage. (**a**) We focus on two specific nodes, SDJ (right), who, under max-flow, is among the early supplied nodes ($\mathbb{S}_{SDJ} = 0.2$), and CGQ (left), representing the majority of undersupplied destinations ($\mathbb{S}_{CGQ} = 3 \times 10^{-3}$). (**b**) Therapeutic availability $q_n(t)$ vs. t at CGQ (blue) as obtained under max-flow dissemination. Due to the sequential nature of this dissemination scheme, the therapeutic reaches CGQ too late, and consequently its infection level $j_n(t)$ remains high, both without (red) and under the effect of max-flow mitigation (yellow). (**c**) In contrast, SDJ is among the first to fill its demand, hence the sharp rise in $q_n(t)$ at an early stage (blue). As a result this node benefits from highly efficienct mitigation, with $r_n(t \to \infty)$ reduced dramatically from 80% (unmitigated, red) to a mere 15% (mitigated, yellow). The challenge is that while CGQ is representative of the majority of destinations, the highly benefited SDJ belongs to a highly exclusive minority and hence cannot represent the typical mitigation efficiency. (**d**,**e**) Egalitarian generates a homogeneous supply pattern, hence now both CGQ and SDJ share a similar (low) supply rate of $\sim 10^{-3}$. Still, they both benefit from a near perfect mitigation (unmitigated—red; mitigated – green). This is thanks to the fact that despite their *equal but slow* supply, they now both begin to receive the therapeutic at an early stage ($q_n(t)$, blue). Indeed, even SDJ, who is now, under egalitarian, experiencing a dramtic drop in its supply rate, from 0.2 to 10^{-3}, continues to benefit from highly efficient mitigation. Hence, the simulataneous, albeit uniformly slow, treatment afforded via egalitarian, not only benefits the max-flow deprived majority, but also continues to effectively treat the superflous minority. (**f**) The global consumption $Q(t)$ vs. t, approaching unity, i.e. all demands are filled, when $t \to \infty$. (**g**) Global mitigation efficiency E vs. the volume of disseminated therapeutics Q. Under max-flow we have $E \to 1$ only in the limit $Q \to 1$ (yellow), i.e. supplying the entire global demand. In contrast, egalitarian has $E \sim 1$ already at $Q \sim 0.1$, achieving, thanks to its concurrent supply patterns, an almost perfect mitigation with only 10% of the resources.

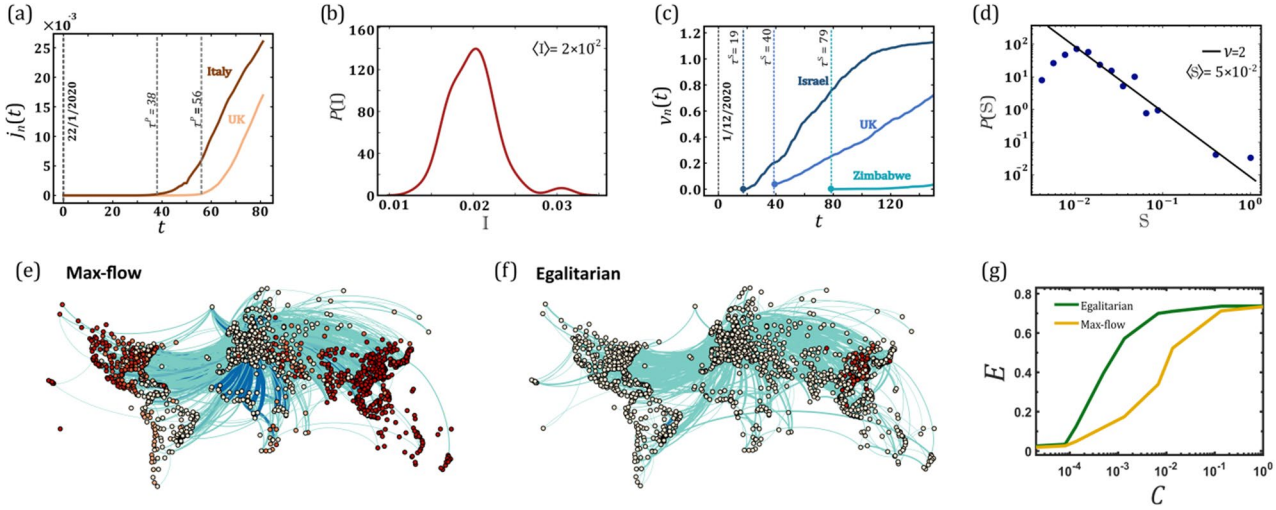

Figure 5. Vaccine and drug-based mitigation of COVID-19. (**a**) To track the SARS-CoV-2 spreading patterns we collected data on $j_n(t)$ vs. t from the intial stages of the pandemic in 41 countries. Fitting each curve to a shifted exponential of the form $j_n(t) \sim e^{\chi_n(t-\tau_n^{\mathrm{P}})}$ we were able to exract the observed COVID-19 infection rate (χ) and delay time (τ^{P}) in each destination (Supplementary Section 6). We set $t = 0$ at the date of the intial outbreak in Wuhan, China (January 22, 2020). This allows us to extract the local infection rate $\mathbb{I}_n = 1/\tau_n^{\mathrm{P}}$, as appears in Eq. (8). Here we show the results for two selected coutries, Italy and UK. (**b**) The infection rate distribution $P(\mathbb{I})$ vs. $\mathbb{I}$. As predicted, we observe a bounded distribution, which translates to a homogeneous spreading pattern. (**c**) We tracked the vaccine rollout $v_n(t)$ in 229 countries (three examples shown here). In each country the vaccination campaign begins at τ_n^{S} (dot), allowing us to evaluate the country's supply rate via $\mathbb{S}_n = 1/\tau_n^{\mathrm{S}}$, as in Eq. (9). Here $t = 0$ represents the time of first vaccine shipment (December 1, 2020). (**d**) $P(\mathbb{S})$ vs. $\mathbb{S}$ as obtained from COVID-19 vaccination data. We observe a power-law of the form of Eq. (10) with $\nu = 2$, precisely our predicted supply patterns. This confirms our thoeretical analysis, showing that indeed, pathogens spread homogeneously, while supplies (here vaccines) spread extremely heterogeneously. (**e**,**f**) We tracked drug distrbution via max-flow (**e**) and egalitarian (**f**) against the spread of COVID-19 (Supplementary Section 6). The total number of infections $r_n(t)$ at $t = 150$ days is represented by red color depth, and the flux of therapeutics along each route by blue. Here we set the outbreak node o to Wuhan, China and the source node s to Brussles, Belgium, one of the distribution sources of the Pfizer-BioNTech COVID-19 vaccine; capacity was set at $C = 5 \times 10^{-3}$. As expected, we find, by comparing the amound of red nodes, that egalitarian supercedes max-flow. (**g**) Efficiency E vs. capacity C as obtained from simulations of COVID-19, show the systematic advantage of egalitarian (green) over max-flow (yellow).

Still, despite these distinctions, our main observation on the supply/demand discrepancy, i.e. Figure 3, remains relevant also in the case of COVID-19. To demonstrate this, we collected data on the spread of both the SARS-CoV-2 virus[41] and the vaccines[42] across different countries. We then evaluated the infection/supply rates $\mathbb{I}_n$ and $\mathbb{S}_n$ of Eqs. (8) and (9) by extracting the delays in the first penetration of the virus, and in the kickoff of the vaccine rollout at each location (Supplementary Section 6). As predicted, we find that $P(\mathbb{I})$ is bounded, capturing a homogeneous spread of the virus, while $P(\mathbb{S})$ is fat-tailed, well-approximated by Eq. (10) with $\nu = 2$, precisely following our prediction (Fig. 5a–d).

This mismatch between the two spreading patterns, and specifically our quantitatively accurate prediction of $P(\mathbb{S})$, captures the heart of our theoretical analysis, motivating the need for our egalitarian dissemination strategy. Hence, while our modeling framework is to some extent stylized, factoring out many of the evident complexities observed in real-world pandemics, these empirical observations offer a crucial testament to the practical relevance of our strategy beyond its *clean* model assumptions.

With several new COVID-19 drugs[31] at different stages of development, we are now offered an opportunity to change route, and revisit our mitigation strategy. Observing the extreme inequality in our de facto vaccine distribution (Fig. 5d), it is crucial that we do not recover similar dissemination patterns with the upcoming drug shipments. To examine the playout of our shipping protocols in this realistic setting, we repeated the simulations of Fig. 2, this time using the COVID-19 disease cycle instead of SIR. Hence, we now use a four-state compartmental model, susceptible, exposed, infected, recovered (SEIR), with transition rates[43,44] adjusted to fit the data collected on the spread of SARS-CoV-2 (Supplementary Section 6). Our results clearly indicate that, similarly to our hypothetical SIR scenario, the COVID-19 therapeutics should also be delivered as evenly as possible (Fig. 5e–g).

Box I: Modeling the mitigation of a global epidemic. In a network of N coupled nodes $n = 1, \ldots, N$, each with a population of M_n individuals, we use the SIR model to track the fraction of M_n who are susceptible (s_n), infected (j_n) or removed (r_n). The infected are divided as $j_n = j_n^{\mathrm{T}} + j_n^{\mathrm{U}}$, among the treated (T) individuals, who have been provided a therapeutic and the untreated (U) individuals, who have not yet gained access to it. The epidemic dynamics is driven by (Supp. Sec. 1)

$$\frac{\mathrm{d}s_n}{\mathrm{d}t} = -\alpha s_n^{\mathrm{U}} j_n \sigma\left(j_n\right) + \sum_{m=1}^{N} A_{nm}(s_m - s_n)$$

$$\frac{\mathrm{d}j_n^{\mathrm{U}}}{\mathrm{d}t} = \alpha s_n j_n \sigma\left(j_n\right) - \beta j_n^{\mathrm{U}} - \rho(q_n) j_n^{\mathrm{U}} + \sum_{m=1}^{N} A_{nm}\left(j_m^{\mathrm{U}} - j_n^{\mathrm{U}}\right)$$

$$\frac{\mathrm{d}j_n^{\mathrm{T}}}{\mathrm{d}t} = -\zeta j_n^{\mathrm{T}} + \gamma \rho(q_n) j_n^{\mathrm{U}} + \sum_{m=1}^{N} A_{nm}\left(j_m^{\mathrm{T}} - j_n^{\mathrm{T}}\right)$$

$$\frac{\mathrm{d}r_n^{\mathrm{U}}}{\mathrm{d}t} = \beta j_n^{\mathrm{U}} + \zeta j_n^{\mathrm{T}} + \sum_{m=1}^{N} A_{nm}\left(r_m^{\mathrm{T}} - r_n^{\mathrm{T}}\right), \tag{16}$$

where α is the infection rate, β is the mortality/recovery rate of the untreated individuals and $\zeta > \beta$ is the recovery rate under treatment. The epidemic reproduction number $\mathcal{R}_0 = \alpha/\beta$ captures the level of contagion of the (untreated) disease. The therapeutic consumption rate $\rho(q_n)$ depends on the availability of the therapeutic $q_n(t)$ in n, as

$$\rho\left(q_n\right) = \min\left\{\frac{q_n(t)}{j_n^{\mathrm{U}}(t)}, 1\right\}. \tag{17}$$

Hence $\rho(q_n)$ increases linearly with $q_n(t)$ as long as the demand (denominator) exceeds the supply. It then saturates to unity when n has excess quantities of the therapeutic, avoiding overconsumption (Supp. Sec. 1.2). The availability $q_n(t)$ is determined by our dissemination scheme, following either max-flow, as in Eq. (3), or egalitarian flow, as in Eq. (11).

In (16) we introduce an invasion threshold ε through the sigmoidal function

$$\sigma\left(j_n\right) = \frac{\left(j_n/\varepsilon\right)^h}{\left(j_n/\varepsilon\right)^h + 1}, \tag{18}$$

which activates the local SIR dynamics only when the local infection levels $j_n = j_n^{\mathrm{U}} + j_n^{\mathrm{T}}$ exceed ε (Supp. Sec. 1.1). The diffusion of individuals between nodes is mediated by A_{nm}, derived from the empirical international air-travel network (Supp. Sec. 2.1).

Discussion

Commodity flow problems are at the heart of many crucial applications, from communications to supply-chains, seeking to optimize a network's capacity to distribute information or goods[20–25,45–47]. Most often the target optimization function, *e.g.*, max-flow, arises naturally from the purpose of the distribution. However, in the context of disease mitigation, the optimization is a consequence not just of the dissemination scheme, but also of its interplay with the viral spread. Indeed, our true goal is not just distribution efficiency in and of itself, but rather *mitigation* efficiency. Hence, to assess a dissemination protocol we must couple it with the spread of the epidemic, and observe its effectiveness in terms of the actual observed reduction in infection levels. Here we have shown that the naïve approach of maximizing the commodity flow fails this test, indeed, providing rapid supply, but at the same time a highly inefficient mitigation. On the other hand—optimizing for homogeneity dramatically improves mitigation efficiency.

Our methodological analysis, and its rather dramatic results, were obtained on a hypothetical scenario, in which the spread is driven by SIR dynamics, the mitigation is based on pre-existing drug supplies, and no additional restrictions, such as lockdowns or travel bans, are employed. This allowed us to focus on the unique impact of our dissemination strategy, removing all additional factors that may impact the spread. In reality, as COVID-19 has demonstrated, real-world pandemics are potentially more complex, both in terms of the disease cycle (SEIR), the disseminated commodity (vaccine) and the social response (distancing, travel restrictions). This will likely require specific adaptations to our methodological idea, but as Fig. 5 clearly indicates—in its essence the egalitarian advantage remains equally relevant also in this more complex setting. Additional practical considerations, such as the potential existence of multiple distribution sources, or the fact that the shipping network may be diverted or restructured for the specific mitigation requirements, are examined in Supplementary Section 5.

Battling a global spread, it is crucial to appropriately set the demands $D_n(t)$, which determine how much supply will be shipped to each node. On the side of caution, the natural tendency is to overestimate these demands, i.e. generate redundancy. However, in the face of a globally spreading epidemic, where the distribution network is stretched to its maximal capacity, such strategy may over-allocate resources to some destinations, while depriving

others. This is, in fact, currently observed as countries are securing excess amounts of COVID-19 vaccine doses at the expense of others[48]. On the other hand, fine-tuning the demands to meet the exact supply gap of each node, as we do, for example in our *urgency-based* strategy, is highly complex, not always practical, and, if inaccurate, may lead to undersupply in some destinations. Our egalitarian optimization addresses this trade-off quite naturally, by simultaneously supplying all nodes. To understand this consider two nodes n and m. Under max-flow, supply will be typically sequential, *e.g.*, n and then m. Under these conditions, overestimating $D_n(t)$ will lead to the shipment of more doses to n, thus wrongly delaying the treatment of m. In contrast, such discrepancy under egalitarian, will have no bearing on m, as both nodes are simultaneously supplied from the start. This makes egalitarian highly robust against the specific assignment of $D_n(t)$, allowing us to design a simple dissemination protocol, free of the need to accurately tailor and fine-tune all demands.

Our analysis focuses on drug-based mitigation, and—in and of itself—has limited relevance to vaccine distribution. The main difference is that vaccines—a preemptive mitigator—are supplied to the susceptible population, while drugs are administered to the infected. As Fig. 4 indicates, this distinction is crucial. Indeed, at any given point in time, since only a small part of the population is infected ($j_n(t)$), a slow but equal drug supply can help suppress the disease in the vast majority of nodes, curing not just the currently infected, but also all their future secondary infections. In simple terms, all nodes benefit thanks to the equality, and practically none pay a significant price because of the resulting slowdown in supply rates. This, however, is not the case regarding the susceptible population, which at the early stages of the disease follow $s_n(t) \sim 1$, i.e. almost all individuals require a vaccine dose. Hence, the egalitarian benefit in which all nodes receive the vaccines, is potentially undermined by the subsequently constricted supply rates. Consequently, while egalitarian continues to outperform max-flow, the margin in vaccine distribution is not nearly as dramatic as the one observed under drug-based mitigation (Supplementary Section 5).

Despite the above, there are many additional considerations in favor of distribution equality, that are not covered by our current modeling framework[48,49]. For example, the risk of vaccine evading mutations is dramatically increased in countries with low vaccine coverage, in which vaccinated and unvaccinated individuals continuously interact[50]. We, therefore, believe, that on top of the results shown here, the call for distribution equality—in drugs or vaccines—should be our main guideline in battling COVID-19 or any future global health crisis.

Our analysis focuses solely on the mitigation efficiency, yet its conclusions touch upon the ethics of resource allocation during a global emergency. While often one is confronted with a clash of values in such cases, here we find it encouraging that efficiency and equity are, in fact, compatible—representing a case in which scientific results go hand in hand with moral directives.

Data availability

All data and code to reproduce and improve our analysis is freely available via: https://figshare.com/account/home#/projects/139465.

Received: 3 January 2021; Accepted: 28 April 2022
Published online: 21 June 2022

References

1. Pastor-Satorras, R. & Vespignani, A. Epidemic spreading in scale-free networks. *Phys. Rev. Lett.* **86**, 3200–3203 (2001).
2. Pastor-Satorras, R., Castellano, C., Van Mieghem, P. & Vespignani, A. Epidemic processes in complex networks. *Rev. Mod. Phys.* **87**, 925–958 (2015).
3. Barzel, B. & Barabási, A.-L. Universality in network dynamics. *Nat. Phys.* **9**, 673–681 (2013).
4. Colizza, V. & Vespignani, A. Epidemic modeling in metapopulation systems with heterogeneous coupling pattern: Theory and simulations. *J. Theor. Biol.* **251**, 450–467 (2008).
5. Apolloni, A., Poletto, C., Ramasco, J. J., Jensen, P. & Colizza, V. Metapopulation epidemic models with heterogeneous mixing and travel behaviour. *Theor. Biol. Med. Model.* **11**, 3 (2014).
6. Tizzoni, M. *et al.* On the use of human mobility proxies for modeling epidemics. *PLoS Comput. Biol.* **10**, 1003716 (2014).
7. Rossman, H. *et al.* A framework for identifying regional outbreak and spread of COVID-19 from one-minute population-wide surveys. *Nat. Med.* **26**, 634–638 (2020).
8. Wu, F. *et al.* A new coronavirus associated with human respiratory disease in China. *Nature* **579**, 265–269 (2020).
9. Chinazzi, M. *et al.* The effect of travel restrictions on the spread of the 2019 novel coronavirus (COVID-19) outbreak. *Science* **368**, 395–400 (2020).
10. Xu, B. *et al.* Epidemiological data from the COVID-19 outbreak, real-time case information. *Sci. Data* **7**, 1–6 (2020).
11. Zhang, J. *et al.* Evolving epidemiology and transmission dynamics of coronavirus disease 2019 outside Hubei province, China: A descriptive and modelling study. *Lancet Infect. Dis.* **20**, 793–802 (2020).
12. Dong, E., Du, H. & Gardner, L. An interactive web-based dashboard to track COVID-19 in real time. *Lancet. Infect. Dis* **20**, 533–534 (2020).
13. Brockmann, D. & Helbing, D. The hidden geometry of complex, network-driven contagion phenomena. *Science* **342**, 1337–1342 (2013).
14. Sattenspiel, L. & Dietz, K. A structured epidemic model incorporating geographic-mobility among regions. *Math. Biosci.* **128**, 71–91 (1995).
15. Hacohen, A., Cohen, R., Efroni, S., Barzel, B. & Bachelet, I. Digitizable therapeutics for decentralized mitigation of global pandemics. *Sci. Rep.* **9**, 14345 (2019).
16. Pastor-Satorras, R. & Vespignani, A. Immunization of complex networks. *Phys. Rev. E* **65**, 036104 (2002).
17. Oles, K., Gudowska-Nowak, E. & Kleczkowski, A. Understanding disease control: Influence of epidemiological and economic factors. *PLoS ONE* **7**, 1–9 (2012).
18. Arinaminpathy, N. & McLean, A. Antiviral treatment for the control of pandemic influenza: some logistical constraints. *J. R. Soc. Interface* **5**, 545–553 (2008).
19. Woolley-Meza, O. *et al.* Complexity in human transportation networks: A comparative analysis of worldwide air transportation and global cargo-ship movements. *Eur. Phys. J. B* **84**, 589–600 (2011).
20. Ahuja, R. K., Magnanti, T. L. & Orlin, J. B. *Network Flows: Theory, Algorithms, and Applications* (Prentice Hall, 1993).

21. Dai, W., Zhang, J. & Sun, X. On solving multi-commodity flow problems: An experimental evaluation. *Chin. J. Aeronaut.* **30**, 1481–1492 (2017).
22. Barnhart, C., Krishnan, N. & Vance, P. H. Multicommodity Flow Problems. In *Encyclopedia of Optimization* 1583–1591 (Springer US, 2001).
23. Fleischer, L. K. Faster algorithms for the quickest transshipment problem. *SIAM J. Optim.* **12**, 18–35 (2001).
24. Ford, L. R. & Fulkerson, D. R. Maximal flow through a network. In *Classic Papers in Combinatorics* 243–248 (Birkhäuser Boston, 2009).
25. Goldberg, A. V. & Tarjan, R. E. Efficient maximum flow algorithms. *Commun. ACM* **57**, 82–89 (2014).
26. Harush, U. & Barzel, B. Dynamic patterns of information flow in complex networks. *Nat. Commun.* **8**, 2181 (2017).
27. Hens, C., Harush, U., Haber, S., Cohen, R. & Barzel, B. Spatiotemporal signal propagation in complex networks. *Nat. Phys.* **15**, 403–412 (2019).
28. Brockmann, D., Hufnagel, L. & Geisel, T. The scaling laws of human travel. *Nature* **439**, 462–465 (2006).
29. Zhang, X., Ruan, Z., Zheng, M., Barzel, B. & Boccaletti, S. Epidemic spreading under infection-reduced-recovery. *Chaos Solitons Fractals* **140**, 110130 (2020).
30. Stegmaier, T., Oellingrath, E., Himmel, M. & Fraas, S. Differences in epidemic spread patterns of norovirus and influenza seasons of Germany: An application of optical flow analysis in epidemiology. *Sci. Rep.* **10**, 14125 (2020).
31. Ledford, H. Dozens of coronavirus drugs are in development—What happens next?. *Nature* **581**, 247 (2020).
32. Barrat, A., Barthelemy, M. & Vespignani, A. *Dynamical Processes on Complex Networks* (Cambridge University Press, 2008).
33. Cohen, J. Designer antibodies could battle COVID-19 before vaccines arrive. *Science.* (2020).
34. Régnier, S. A. & Huels, J. Drug versus vaccine investment: A modelled comparison of economic incentives. *Cost Eff. Resour. Alloc.* **11**, 23 (2013).
35. Cenciarelli, O. *et al.* Ebola virus disease 2013–2014 outbreak in west Africa: An analysis of the epidemic spread and response. *Int. J. Microbiol.* **2015**, 769121 (2015).
36. WHO | Statement on the 1st meeting of the IHR Emergency Committee on the 2014 Ebola outbreak in West Africa. (WHO, 2014). http://www.who.int/mediacentre/news/statements/2014/ebola-20140808/en/.
37. Barzel, B. & Barabási, A.-L. Network link prediction by global silencing of indirect correlations. *Nat. Biotechnol.* **31**, 720–725 (2013).
38. Barzel, B. & Biham, O. Quantifying the connectivity of a network: The network correlation function method. *Phys. Rev. E* **80**, 46104–46115 (2009).
39. Emanuel, E. J. *et al.* Fair allocation of scarce medical resources in the time of Covid-19. *N. Engl. J. Med.* **382**, 2049–2055 (2020).
40. Laventhal, N. *et al.* The ethics of creating a resource allocation strategy during the COVID-19 pandemic. *Pediatrics* **146**, (2020).
41. DonDong, E., Du, H. & Gardner, L. An interactive web-based dashboard to track COVID-19 in real time. *Lancet Infect. Dis.* **20**, 533 (2020).
42. https://ourworldindata.org/covid-vaccinations?country=OWID_WRL.
43. Meidan, D. *et al.* Alternating quarantine for sustainable epidemic mitigation. *Nat. Commun.* **12**, 220 (2021).
44. Bar-On, Y. M., Flamholz, A., Phillips, R. & Milo, R. SARS-CoV-2 (COVID-19) by the numbers. *Elife* **9**, e57309 (2020).
45. Ford, L. R. & Fulkerson, D. R. Constructing maximal dynamic flows from static flows. *Oper. Res.* **6**, 419–433 (1958).
46. Fleischer, L. & Skutella, M. Quickest flows over time. *SIAM J. Comput.* **36**, 1600–1630 (2007).
47. Aronson, J. E. A survey of dynamic network flows. *Ann. Oper. Res.* **20**, 1–66 (1989).
48. Callaway, E. The unequal scramble for coronavirus vaccines—by the numbers. *Nature* **584**, 506 (2020).
49. Figueroa, J. P. *et al.* Achieving global equity for COVID-19 vaccines: Stronger international partnerships and greater advocacy and solidarity are needed. *PLoS Med.* **18**, e1003772 (2021).
50. Zhang, X. *et al.* A spatial vaccination strategy to reduce the risk of vaccine-resistant variants. Research Square (2021).

Acknowledgements
This work was supported by the Israel Science Foundation (Grant No. 499/19), the bi-national Israel-China ISF-NSFC joint research program (Grant No. 3552/21) and the Bar-Ilan University Data Science Institute grant for COVID-19 related research.

Author contributions
All authors designed and conducted the research. A.H. analyzed the data and conducted the numerical simulations, A.H., B.B. and R.C. lead the analytical derivations, and I.B. and S.E. advised on the biological applicability. B.B. was the lead writer.

Competing interests
The authors declare no competing interests.

Additional information
Supplementary Information The online version contains supplementary material available at https://doi.org/10.1038/s41598-022-12261-x.

Correspondence and requests for materials should be addressed to B.B.

Reprints and permissions information is available at www.nature.com/reprints.

Publisher's note Springer Nature remains neutral with regard to jurisdictional claims in published maps and institutional affiliations.

Open Access This article is licensed under a Creative Commons Attribution 4.0 International License, which permits use, sharing, adaptation, distribution and reproduction in any medium or format, as long as you give appropriate credit to the original author(s) and the source, provide a link to the Creative Commons licence, and indicate if changes were made. The images or other third party material in this article are included in the article's Creative Commons licence, unless indicated otherwise in a credit line to the material. If material is not included in the article's Creative Commons licence and your intended use is not permitted by statutory regulation or exceeds the permitted use, you will need to obtain permission directly from the copyright holder. To view a copy of this licence, visit http://creativecommons.org/licenses/by/4.0/.

© The Author(s) 2022